Three-Phase Soft-Switched Active Rectifier in Grid-Forming Mode for Non-Isolated EV Chargers

Tanner Carlson
Electrical Engineering[redacted]
Columbia University
New York, United States
Email: tanner.carlson@columbia.edu

Manfredi Gangi
Electrical Engineering[redacted]
Columbia University
New York, United States
Email: mg4632@columbia.edu

***Abstract*—Grid-forming inverters are becoming an increasingly common topic in power electronics. Microgrids will be an important component in the future of energy as they allow a consumer to be separated from the traditional grid and the problems accompanying it. Grid-forming inverters can generate a voltage grid without having to lock into an existing one. This behavior introduces potential advantages such as enhanced resiliency and self-reliance. In this paper, two different scenarios of grid-forming converters are simulated. Specifically, the first case involves the use of a grid-forming converter in island mode to supply a load. The second simulation introduces the addition of a secondary grid-following converter, which will lock into the local grid generated by the first GFM device. This process involved modeling not only the physical components of the system but also the control methods used to maintain the stability of the grid. The simulations were performed in PLECS.**

I. Introduction

Blackouts often affect areas far beyond the initial fault in the system. This can be seen in the Northeast blackout of 2003, which affected 40 million people in the US and Canada [1]. Winter Storm Uri in Texas caused another major blackout in 2021. Our current power systems need to be updated, but often, policy gets in the way. There is a push for developing new reliability strategies and devices. Currently, the most common power converter type is grid-following, which only works if attached to an active grid. These types of inverters are not effective for microgrids, blackstart operation, or reliability enhancement.

A modern technology that could mitigate these problems is the grid-forming inverter. This type of inverter can be a "leader," whereas other types of inverters can only follow. GFM inverters are thought of as the leader, as they are capable of establishing frequency and voltage references without a connected grid. This actively controls the amplitude and phase of the output voltage. Grid-following inverters act as followers, where they synchronize to an imposed voltage signal. As photovoltaic and battery systems become more prevalent, grid-forming inverters become increasingly important in maintaining resilience and stability in standalone power systems.

Data center and electric vehicle (EV) adoption are widely expected to increase. These new loads will require energy from the grid, thus further decreasing the reliability of the power system. At the same time, it is true that EVs are often parked, and therefore represent a possible energy source in the form of their batteries from the grid perspective. Thus, adopting a grid-forming converter for the EV onboard charging system would allow the interconnection of the EV battery with the grid and also support the control.

The research into grid-forming inverters may be the key to powering a large load with multiple electric vehicles without the need for a leader-follower relationship. Connecting two or more electric vehicles to a residential load in parallel using CVCF mode causes overcurrent and power sharing. Grid-forming control may be the solution to overcome these limitations and achieve an energy hub [2]. This paper continues to discuss various control methods and the differences that can be seen in grid-following and grid-forming inverters.

Another paper that I found quite useful during this research was the Control of Power Converters in AC Microgrids. Using progressively complicated figures as stepping stones, the diagrams in this paper offer a comprehensive guide on how to create a simulation. This paper also mentions the growing adoption of electric vehicles and battery storage systems. It also offers microgrids as a solution for reliability [7].

Cost and charging time are also significant barriers to the adoption of electric vehicles. "Non-isolated chargers can achieve greater efficiencies and reduce the total costs because the converter can be easily integrated in the drivetrain of the vehicle" [3]. The devices on board are designed for level 2 power ratings (3 to 22 kW). These offer much slower charging than public Level 1 power ratings (30 kW to 360 kW). Research on onboard chargers is crucial. A four-wire configuration with control over the neutral conductor current works with balanced and unbalanced loads [4].

The Grid Forming Inverter Modeling, Control, and Applications paper focused on a general overview of grid-forming techniques. Grid-following inverters need a grid to set voltage and frequency, while the grid-forming inverters set their output. This is how we can operate our first working simulation without a connected device. Various control strategies are discussed in this paper that may be good progressions of our design, such as droop control or synchronous machine-based control [5].

This paper investigates using a three-phase onboard EV charger as a grid-forming converter device. Among the differ-

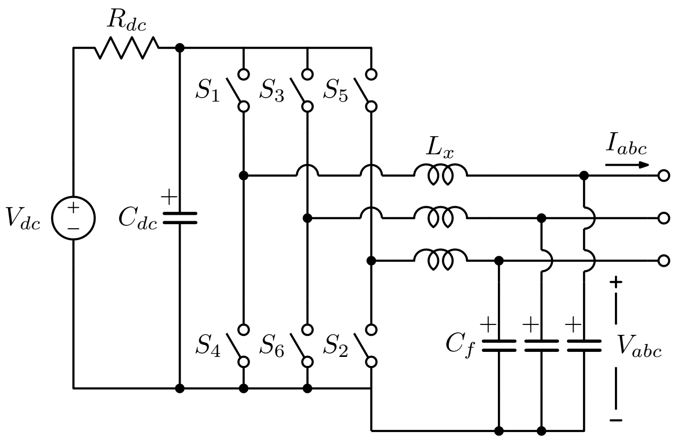

Fig. 1. Inverter topology

ent control strategies, this analysis introduces the regulation algorithms for island mode inverters, where only one device can be the actual leader. All other converters have to connect as followers through the use of PLL algorithms. Two different PLECS simulation results are described. The first one demonstrated the functionality of the device in island mode while supplying real power from the EV battery to a load. The second one also introduces the effect of the connection of a grid-following converter through a PLL algorithm, with the final goal of charging the battery of the second EV while still supplying power to the original load.

II. System Under Investigation

Fig. 1 shows the topology of the inverter. The values of the various components can be seen in Fig. 2. A notable value includes the V_{dc} of 800 volts, which represents a battery. The C_{dc} serves as a means to reduce the ripple of the V_{dc} voltage caused by the switches. The switches are MOSFETs in the simulation and are controlled by the formulated duty cycle. The final stage is an LC filter, which serves to reduce high-frequency harmonics and shape the sinusoidal outputs at the terminals. Both V_{abc} and I_{abc} are being measured from this circuit. The voltage is measured over the output capacitor C_f, and contains an a, b, and c component. The same is true of the current, except this is measured after the capacitor.

There are two simulations formulated for this paper. The first is a three-phase controlled it in island mode to supply power from the EV battery to the three-phase load. Fig. 2 shows this PLECS simulation, barring the details of the transform subsystems. The second is an extension of the island mode GFM inverter with the addition of a PLL-connected device. Fig. 5 is a simplified circuit diagram of the more advanced simulation. Later in the paper, a more detailed version can be seen in Fig. 6, the PLECS simulation circuit.

A. Clarke-Park mathematical transformations

In the first simulation, a three-phase V_{gen} value is generated for control purposes. These voltages are sinusoidal and represent the power grid voltages with a 400 V offset. The

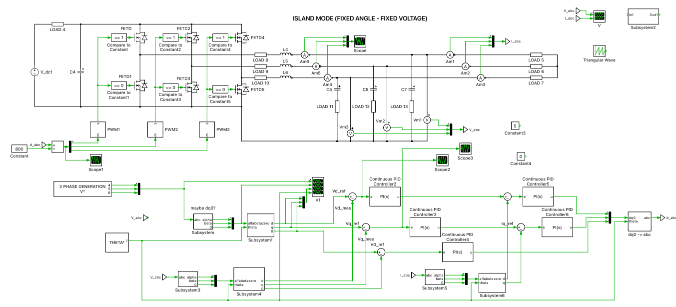

Fig. 2. Island mode grid-forming inverter

way we control the circuit using this voltage generation is by transforming it into DC values that are easily followed by PI devices. These transformations in my simulation are necessary for proper control.

Two transforms commonly used together are famously known as the Clarke-Park transform. The Clarke transform first changes the voltage (a, b, c) values to $(\alpha, \beta, 0)$. The Park transform takes this a step further by rotating the reference frame, allowing the controls for inverters to be simplified [6]. Fig. 3 shows the reference signals, transformations, and theta value. After the Clarke transform, the waveforms are $\frac{\pi}{2}$ or $90°$ out of phase with each other. After the Park transform, the $(d, q, 0)$ values are all DC, which allows for the voltage controller to follow a DC rather than a sinusoid. Finally, the theta value is the angle of rotation used in the Park transform. It is based on a frequency of 50 hertz. The linear behavior confirms that this is a grid-forming application rather than grid-following. The results of these transforms can be seen in Fig. 3.

1) Clarke matrix: The Clarke transformation projects the three-phase (a, b, c) quantities onto a stationary orthogonal frame $(\alpha, \beta, 0)$.

$$\begin{bmatrix} v_\alpha \\ v_\beta \\ v_0 \end{bmatrix} = \sqrt{\frac{2}{3}} \begin{bmatrix} 1 & -\frac{1}{2} & -\frac{1}{2} \\ 0 & \frac{\sqrt{3}}{2} & -\frac{\sqrt{3}}{2} \\ \frac{1}{\sqrt{2}} & \frac{1}{\sqrt{2}} & \frac{1}{\sqrt{2}} \end{bmatrix} \begin{bmatrix} v_a \\ v_b \\ v_c \end{bmatrix} \tag{1}$$

2) Park matrix: The Park transformation rotates the $(\alpha, \beta, 0)$ frame into the synchronous rotating frame $(d, q, 0)$ using the reference angle θ:

$$\begin{bmatrix} v_d \\ v_q \\ v_0 \end{bmatrix} = \begin{bmatrix} \cos\theta & \sin\theta & 0 \\ -\sin\theta & \cos\theta & 0 \\ 0 & 0 & 1 \end{bmatrix} \begin{bmatrix} v_\alpha \\ v_\beta \\ v_0 \end{bmatrix} \tag{2}$$

Implementing these Clarke-Park transforms with blocks in PLECS creates intricate designs for a seemingly simple task. One of the areas to pay attention to is the transformation back to (a, b, c) from the new $(d, q, 0)$ values. It is tricky, as the calculations are in reverse. These (a, b, c) values are important for generating the PWM signals that will switch the MOSFETs on the inverter. As seen in Fig. 3, displaying these transformations, the control system can operate with DC signals rather than sinusoidal waveforms.

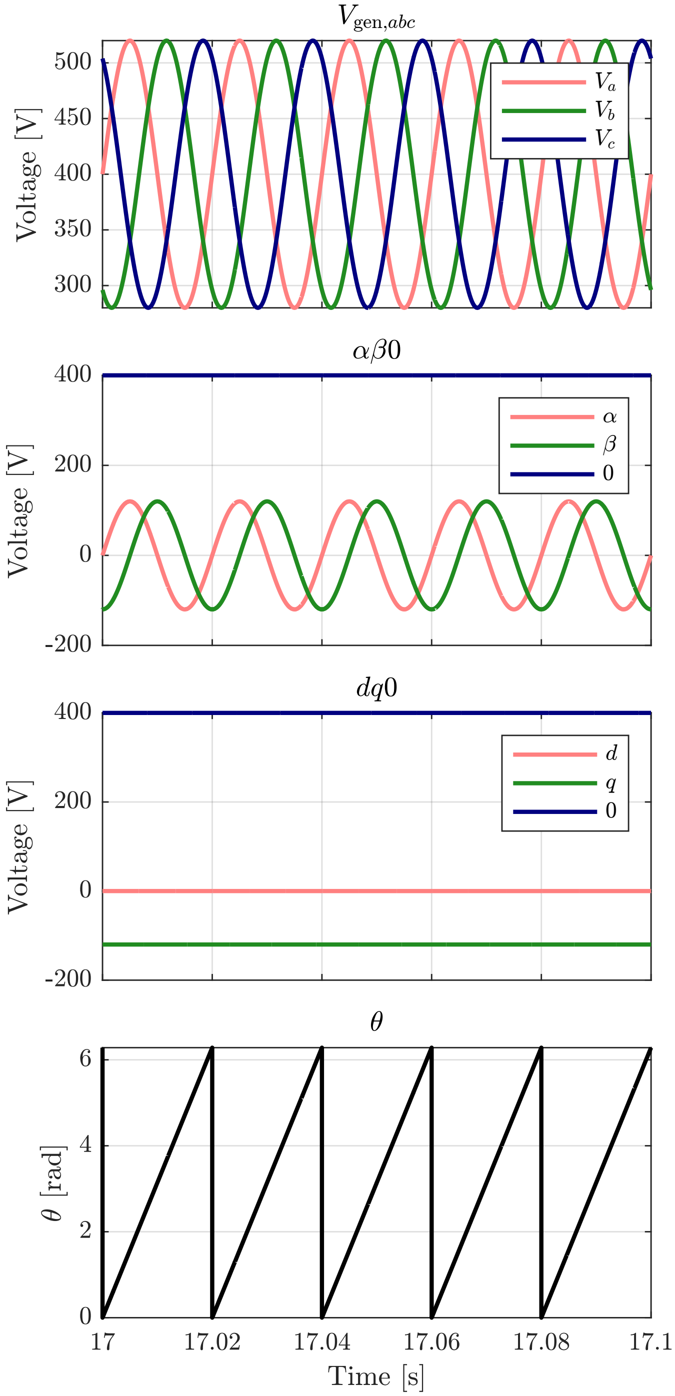

Fig. 3. Signals following the Clarke-Park transform

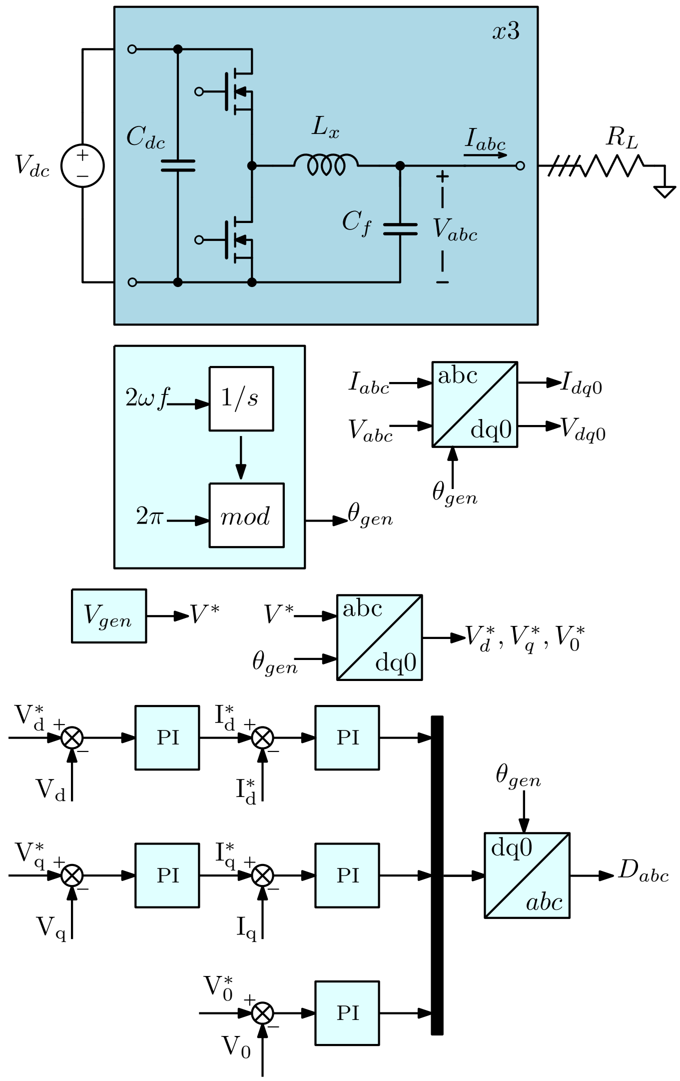

Fig. 4. Control for the inverter switches

Fig. 4 shows an in-depth guide on the development of the duty cycle for the switches. The measurements of the device are taken from the same areas discussed earlier. These measurements, combined with the reference signals, formulate the duty cycle. First, we generate the three-phase V_{gen} values along with the theta used for the transforms. The theta is calculated by combining the integration of $2\omega f$ and 2π using a mod block. This gives θ_{gen}, which is used in the Clarke-Park transformations.

The generated values V_d^*, V_q^*, V_0^* are compared with the measured values V_d, V_q, V_0. After subtracting the measured voltages from the generated ones, these signals are processed through the PI. The proportional component is concerned with the error, while the integral component compounds the interest of this error over time. Some of the PIs in this case are being used as a voltage controller, while others are used to control current. It is beneficial to use these as they are relatively simple and useful.

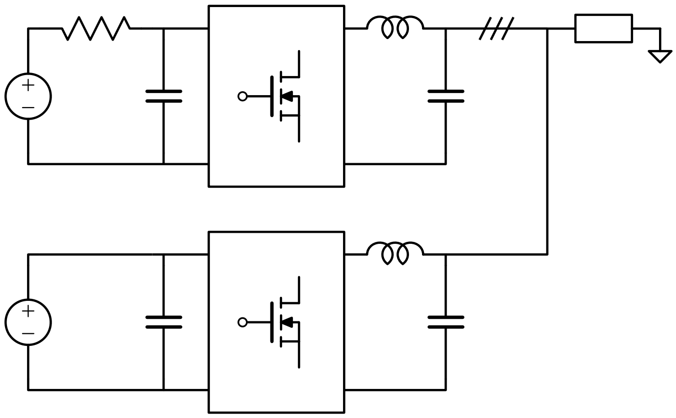

Fig. 5. Simplified circuit diagram

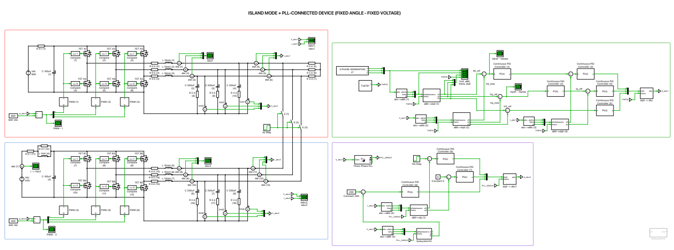

Fig. 6. Advanced simulation

After the signals are processed through the control scheme, the output is used to modulate the pulse width of the PWM signal. The pulse-width modulation controls the switching of the MOSFETs, and therefore, the sinusoidal output at the terminals seen in Fig. 1.

B. Isolated grid-forming inverter

The first case of our simulation represented a GFM island mode inverter. It used the control scheme previously described to produce a sinusoidal output at the R_L loads. In this simulation, the theta value was fixed based on a frequency of fifty hertz. This model also employs the control system seen in Fig. 4. Another aspect of this simulation was the three-phase LC filter. The combination of these components smoothes the waveform before it is dissipated in the load. The capacitor closest to the DC source acts as a filter for the voltage ripple from the switching of the inverter.

C. Isolated grid-forming inverter with attached PLL device

The more advanced version of the project came from developing upon the first. The modular system is beneficial for troubleshooting and understanding the roles of the different parts of the topology. This simulation still has the same aspect of the grid-forming inverter, but now has a second device that follows. The result of this secondary device is to transfer power from V_{dc1} to V_{dc2} or vice versa. A simplified version of the circuit can be seen in Fig. 5, while the PLECS simulation can be inspected with Fig. 6.

The second inverter has a battery that is half the size of the original, possibly representing an electric vehicle. Table I shows some important variables chosen for the system. Unlike the first inverter operating in grid-forming mode, this second inverter functions in grid-following mode. A PLL (Phase-Locked-Loop) is used to enable this connected device to synchronize with the voltage waveform of the grid-forming inverter. The estimated angle is used to align the internal reference frame of the inverter with the grid voltage. The PLL enables the second inverter to accept or push power at the correct phase and frequency.

TABLE I
KEY CONTROL AND SYSTEM PARAMETERS

Parameter	**Symbol/Name**	**Value**
DC Link Voltage	V_{dc1}	800 V
Output Frequency	f	50 Hz
Carrier Frequency	f_{carrier}	100 kHz
Battery Voltage	V_{dc2}	400 V

III. Results

To analyze the results, the data from PLECS was exported and represented using MATLAB. Another key aspect of the simulation not previously mentioned includes the steps. The switch connects the second device to the grid-forming inverter at five seconds, and the PLL-connected device begins tracking a power reference of $-16\sqrt{2}$ amps at ten seconds. This allows for the second device to be connected and settle, and then for the power transfer to start happening. Since the value utilized on the step is negative, the power is pushed from the first device to the second. A positive value here would result in the opposite flow of current.

The first two plots in Fig. 7 displays the output voltage and current ($V_{\text{abc,1}}$ and $I_{\text{abc,1}}$) of the grid-forming inverter measured at the terminals. The voltage control loop is working properly as the waveforms are sinusoidal and shifted by $\frac{2\pi}{3}$ rad or $120°$. All three phases have a constant amplitude, which shows the voltage control. The current waveform is promising as it is providing power to the connected load under steady-state conditions. Another important aspect to note is that the steady-state condition before the step at five seconds converges to the V_{gen} values: another indicator that the control is working properly.

Fig. 7 also shows the DC current flowing into the battery source of the connected device. The device is receiving smooth power and steady-state charging shortly after the step at ten seconds. The current starts at zero, as this device is unconnected at the beginning of the simulation. At five seconds, this device is connected, and a ripple in the current is observed. This value oscillates around zero. The more important part of the simulation is after the ten-second step, at which point the V_{dc2} battery begins to charge.

IV. Conclusion

Grid-forming inverters are already becoming more commonly implemented and offered as solutions. These emerging technologies will shape our future energy resources, and it

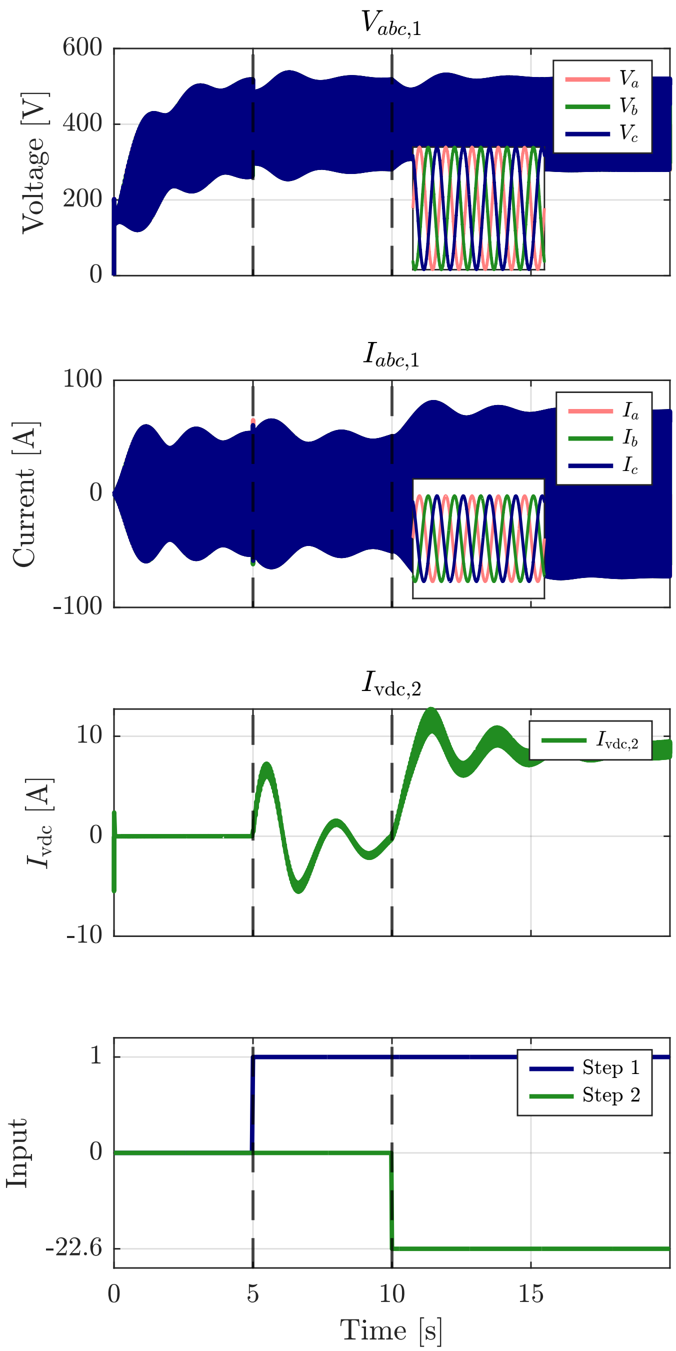

Fig. 7. Simulation results

is important to research them vigorously. There is ongoing research in this area, which is promising. There was no lack of information on this topic. The results of this simulation are promising. It shows that we can easily develop control systems for grid-forming microgrids and connect other devices.

Whether it is adding a fourth leg to the inverter or continuing to develop the control method, there are many things that I would be interested in expanding upon in this project. Some realistic goals would be to implement a better control system, such as droop control, or to test the system under fault conditions. A more unrealistic, yet interesting, expectation would be to implement the simulation into a hardware solution and test it.

V. Acknowledgment

This research report was written for ELEN 6002 in the Spring 2025 semester. The research-based course was taught by [redacted], which included weekly meetings with Manfredi Gangi.

I would like to sincerely thank Manfredi and the Professor for the project. I have deepened my knowledge of power electronics and have gained a great insight from the experience. I feel accomplished that I designed such an intriguing simulation. I would also be interested in continuing the work in the fall.

References

[1] NASA Office of Safety and Mission Assurance, “Powerless: Northeast Blackout of 2003,” *Safety Message*, Mar. 1, 2008. [Online]. Available: https://sma.nasa.gov/docs/default-source/safety-messages/safetymessage-2008-03-01-northeastblackoutof2003.pdf

[2] E. Fayad, D. Sal y Rosas, A. Bruyere, and F. Poirier, “Automotive charger grid-forming control opportunities for G2V and V2X applications,” in *Proc. IEEE Veh. Power Propuls. Conf. (VPPC)*, 2023.

[3] M. Gangi and M. Preindl, “Four-leg soft-switched active rectifier for non-isolated EV chargers,” in *Proc. IEEE Workshop Control Modeling Power Electron. (COMPEL)*, 2024.

[4] M. Gangi and M. Preindl, “Modular soft-switched EV charger with four-leg PFC stage and transformerless on-demand DC/DC configuration,” in *Proc. IEEE Conf. Power Electron. Drive Syst. (PEDS)*, 2023.

[5] D. B. Rathnayake *et al.*, “Grid forming inverter modeling, control, and applications,” *IEEE Access*, vol. 9, pp. 114781–114795, Aug. 2021, doi: 10.1109/ACCESS.2021.3104617.

[6] C. J. O’Rourke, M. M. Qasim, M. R. Overlin, and J. L. Kirtley, “A geometric interpretation of reference frames and transformations: dq0, Clarke, and Park,” *IEEE Trans. Energy Convers.*, vol. 34, no. 4, pp. 2070–2083, Dec. 2019, doi: 10.1109/TEC.2019.2941175.

[7] J. Rocabert, A. Luna, F. Blaabjerg, and P. Rodríguez, “Control of power converters in AC microgrids,” *IEEE Trans. Power Electron.*, vol. 27, no. 11, pp. 4734–4749, Nov. 2012, doi: 10.1109/TPEL.2012.2199334.